

Localized deformation in sands and glass beads subjected to plane strain compressions

Li Zhuang^{*1}, Yukio Nakata^{2b} and In-Mo Lee^{1c}

¹ Civil, Environmental and Architectural Engineering, Korea University, Seoul 136-713, Korea

² Civil and Environmental Engineering, Yamaguchi University, Ube 755-0097, Japan

(Received October 08, 2012, Revised May 14, 2013, Accepted July 23, 2013)

Abstract. In order to investigate shear behavior of granular materials due to excavation and associated unloading actions, load-controlled plane strain compression tests under decreasing confining pressure were performed under drained conditions and the results were compared with the conventional plane strain compression tests. Four types of granular material consisting of two quartz sands and two glass beads were used to investigate particle shape effects. It is clarified that macro stress-strain behavior is more easily influenced by stress level and stress path in sands than in glass beads. Development of localized deformation was analyzed using photogrammetry method. It was found that shear bands are generated before peak strength and shear band patterns vary during the whole shearing process. Under the same test condition, shear band thickness in the two sands was smaller than that in one type of glass beads even if the materials have almost the same mean particle size. Shear band thickness also decreased with increase of confining pressure regardless of particle shape or size. Local maximum shear strain inside shear band grew approximately linearly with global axial strain from onset of shear band to the end of softening. The growth rate is found related to shear band thickness. The wider shear band, the relatively lower the growth rate. Finally, observed shear band inclination angles were compared with classical Coulomb and Roscoe solutions and different results were found for sands and glass beads.

Keywords: plane strain compression; unloading; stress path; particle shape; shear band; DIC analysis

1. Introduction

There are many kinds of unloading projects in the field of civil engineering, such as excavation for retaining walls, slope cutting, tunneling, and preloading and unloading in subgrades. Such excavation or removal of soil (load) will generate a new boundary and the soil around the new boundary will undergo different stress paths accompanied by stress release. Taking the construction of a retaining wall as an example, soil at the bottom of the excavation is subjected to extension as the overburden being removed, and soil behind the wall in active state is subjected to shear compression by the progressive decrease of the lateral pressure while the vertical stress distribution have been shown to have great influence on the common plane strain compression remains constant (Head 1992). Plane strain extension behavior in sands has been investigated by

*Corresponding author, Researcher, E-mail: zhuangli2004@126.com

^a Professor, E-mail: nakata@yamaguchi-u.ac.jp

^b Professor, E-mail: inmolee@korea.ac.kr

several studies (Masuda *et al.* 1999, Röchter *et al.* 2010, 2011) and it is different from plane strain compression behavior. Very few studies have examined the shear stress path under constant axial load and decreasing confining pressure either in triaxial or plane strain test (Chu *et al.* 2012). This stress path is usually load controlled, while the common shear stress path is deformation controlled. Chu and Wanatowski (2009) noted that the two loading modes only affect the post-peak stress-strain behavior of sand, given the other conditions are the same. Compared to post-peak behavior, shear strength and deformation before failure are more important for calculation of excavation problems. Therefore, this behavior and influencing factors are focused in this study.

On the other hand, several important factors such as confining pressure, density, particle size behavior of sands including shear band formations (Alshibli and Sture 2000, Chu and Wanatowski 2009, Chu *et al.* 2012, Desrues and Viggiani 2004, Finno *et al.* 1997, Rechenmacher 2006, Rechenmacher and Finno 2004, Tatsuoka *et al.* 1990, Tejchman *et al.* 2007, Wanatowski and Chu *et al.* 2006, 2010). Most studies agreed that shear banding happens slightly before the peak. However, there appears no consensus for definition of the onset of shear bands. Comparing results of observed shear band inclination angles with classical predictions also varied in those studies. Moreover, particle shape especially surface roughness has been proven to have significant influence on the shear strength of granular materials through experimental tests and DEM simulations (Alshibli and Alsaleh 2004, Cho *et al.* 2006, Sezer *et al.* 2011, Shinohara *et al.* 2000, Katagiri *et al.* 2010, Maeda *et al.* 2010, Matsushima and Chang 2011). Very few studies have considered particle shape effects in plane strain compression test. Alshibli and Sture (2000) compared plane strain shear behavior of fine, middle and coarse sands with rounded to angular particle shapes. However, the observed particle shape effects were mixed with particle size effects.

This paper mainly aims on understanding behavior of granular materials subjected to unloading shear while focusing on particle shape effect. Therefore, four types of material with angular, sub-angular and round particle shapes were used. Three of them have similar particle size distributions. Plane strain compression tests under decreasing confining stress were mainly performed and common compression tests with constant confining stress were also performed to make comparisons. Local deformations including shear bands patterns were investigated using the digital image analysis.

2. Experimental set-up

2.1 Stress paths

Two types of plane strain compression tests under different stress paths were compared in this study, as shown in Fig. 1. p' is the mean effective stress and q is the deviator stress. The first type is load-controlled test under decreasing confining pressure (referred to as PSCD test), where effective confining stress on the specimen, σ'_3 , is decreased before the failure, while the effective axial stress, σ'_1 , remains constant by adjusting displacement of loading platen. The confining pressure was automatically decreased at a rate within 1-3 kPa/min and smaller decrements were taken near failure. When the specimen arrives at failure, confining stress decrease was stopped and shearing was continued under constant axial displacement rate. The second type is the conventional deformation-controlled plane strain compression test (referred to as PSC test), where confining pressure was kept constant and the specimen was sheared under a constant axial displacement rate. During the whole shearing process, the axial displacement rate was kept at 0.1 mm/min. A number of practical problems corresponding to the two different stress paths are

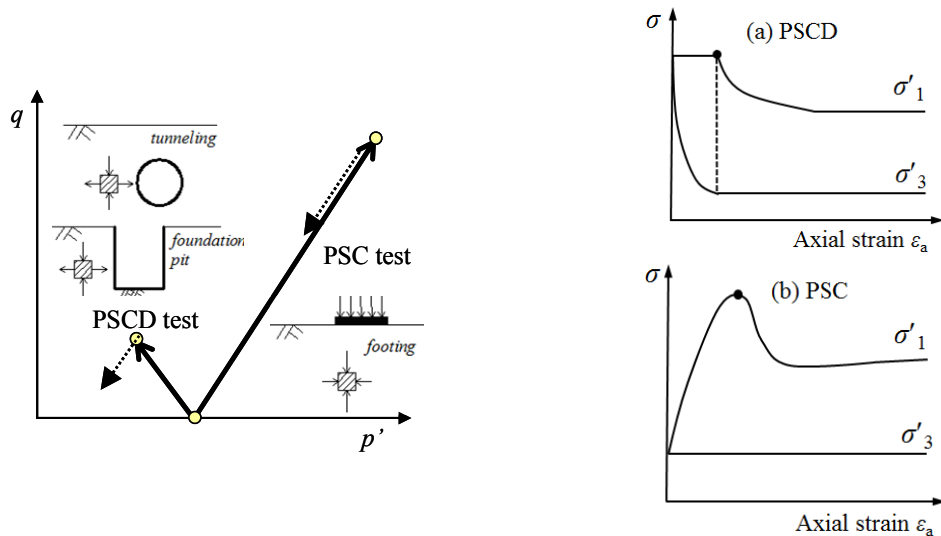


Fig. 1 Two stress paths and principal stress variations in the PSCD and PSC tests

illustrated in the examples given in Fig. 1. The soil element below a footing follows a stress path as in the PSC test, while those located at the lateral sides of excavation of tunnels or foundation pits are closer to the stress path in the PSCD test.

2.2 Test materials and methods

All the tests were performed in a plane strain test apparatus, as shown in Fig. 2. Confining pressure is applied by air and its increase or decrease is controlled by computer program. Confining plate with a transparent glass window is designed for both front and back sides to restrict deformation and to take photographs of specimen. Volumetric change is measured through a burette. Each specimen has approximately a width of 60 mm, a depth of 80 mm, and a height of 160 mm. Loading was applied at the top of the specimen and grease was painted on the front and back of specimen in the direction of zero strain to reduce friction. The bottom end platen is restrained from lateral sliding. The intermediate principal stress cannot be measured in this study (Wanatowski and Chu 2006). Photographs of specimens in the front plane were taken during the shearing process to observe local deformations.

Four types of material consisting of two silica sands and two solid glass beads were used and these are referred to in this paper as Ube No. 6A sand, Toyoura sand, Glassbead1 and Glassbead2, respectively. Their particle size distributions are compared in Fig. 3. The first three types of material have the similar particle size distribution, while the Glassbead2 is quite uniform glass beads with much bigger grain size. The Ube No. 6A sand and Toyoura sand have angular and subangular particles separately, and the two glass beads have the same rounded particles, as shown in the photos taken using scanning electron microscope (SEM) in Figs. 4(a)-(d). It should be noted that not all the particles in Glassbead1 are perfectly round and there is very small amount of defective beads being mixed in most rounded beads. Physical properties of materials are shown in Table 1. The aspect ratio (A_r : the ratio of length to width of a particle) and roundness (R_c : a measure of circularity of a particle; equation given in Table 1) were calculated for particles with its

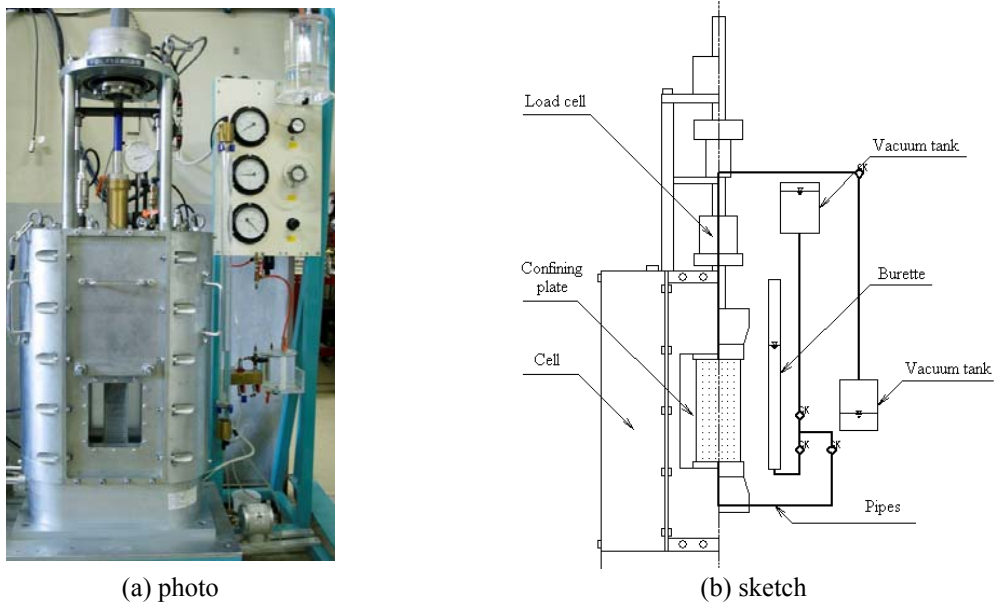
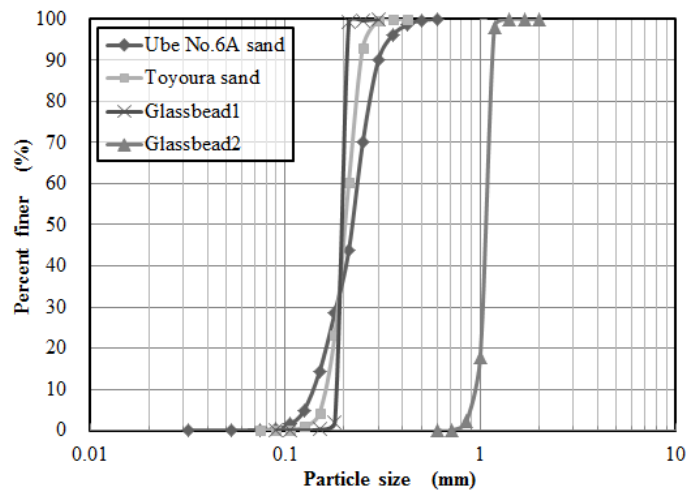


Fig. 2 Plane strain compression test apparatus



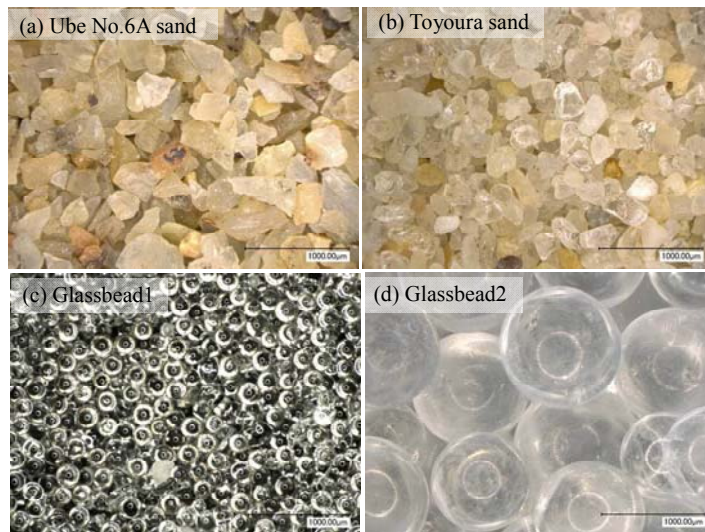


Fig. 4 SEM photos of the four types of material

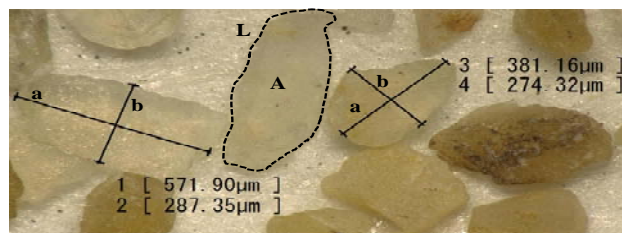


Fig. 5 Measurement of geometry sizes of particles

mean grain size (R_c) in SEM images. Fig. 5 shows an example of how to measure the geometric size of particles.

Air pluviation sampling method was used with a constant drop height of 125 cm. The falling height of 125 cm was the maximum possible manageable distance of the sampling apparatus for the given study. Specimen is divided into 5 layers and the falling height is kept constant for each layer. As a result, the more angular particles produce a looser specimen when the pluviation method is applied under the same drop height. For the maximum possible falling heights, only Ube No.6A sand with the most angular particle shape produced a much lower relative density (around 52%) compared to those of the other three materials. Therefore, a little bit of compaction is done on the Ube No. 6A sand specimen by hitting on the side platens (steel model) of specimen uniformly using a small rubber hammer to prepare denser specimens. However, the final obtained relative density of dense Ube No.6A sand was about 73%, which is approximately lower by 10% compared to those of the other materials.

The initial relative density of specimens produced for the four types of material is ($73\% \pm 1\%$), ($80\% \pm 5\%$), ($80\% \pm 3\%$) and ($88\% \pm 9\%$) respectively. To saturate the specimen, de-aired water was flushed through the specimen and then a back pressure of 50 kPa was applied. All the specimens were isotropically consolidated for 1 hour and then they were sheared until about 12%

Table 2 Summary of test conditions and measured results

Material	Void ratio e_0	Relative density D_r (%)	C.P. (kPa)	Test type	R_{\max}	Mobilized angle ϕ_{\max} (°)	Dilation angle Ψ (°)	θ_p (°)	θ_r (°)	Coulomb-solution (°)	Roscoe solution (°)
Ube No.6A sand	0.735	73.4	50	PSC	9.1	53.3	20.5	70.8	70.8	71.7	55.3
	0.738	72.7	50	PSCD	11.0	56.6	24.2	73.6	68.4	73.2	56.1
	0.734	73.6	100	PSCD	10.0	54.9	23.0	71.1	67.4	72.5	56.5
	0.733	73.9	200	PSCD	9.6	54.4	21.1	70.2	68.0	72.1	55.6
Toyoura sand	0.684	85.6	50	PSC	6.8	48.0	19.2	69.2	69.2	69.0	54.6
	0.72	75.1	50	PSCD	8.7	52.5	18.1	69.3	69.7	71.3	54.2
	0.704	79.8	100	PSCD	8.0	51.1	17.7	68.6	68.9	70.5	53.9
	0.695	82.4	200	PSCD	7.4	49.6	17.7	69.6	70.0	69.8	53.9
Glass bead1	0.6	82.1	50	PSC	4.3	38.5	19.2	56.3	53.8	64.3	54.6
	0.6	82.1	50	PSCD	5.2	42.6	18.3	61.6	58.4	66.3	54.1
	0.607	78	100	PSCD	4.5	39.5	17.8	59.1	56.0	64.8	53.9
	0.61	76.3	200	PSCD	4.2	38.0	16.8	54.6	54.3	64.0	53.4
Glass bead2	0.583	89.8	50	PSC	4.0	36.9	16.2	54.0	51.8	63.4	53.1
	0.596	78.8	50	PSCD	4.5	39.5	15.1	54.5	51.8	64.8	52.6
	0.575	96.6	100	PSCD	3.9	36.3	15.1	53.7	51.8	63.1	52.6
	0.574	97.5	200	PSCD	3.7	35.1	15.1	53.7	51.8	62.5	52.6

* e_0 is the initial void ratio and e_c is the void ratio after consolidation;

θ_p , θ_r are measured inclination angles of the main shear band near the peak and at the end of shearing

axial strain. For each type of material, one PSC test was performed at an initial consolidated pressure $\sigma'_{c0} = 50$ kPa and three PSCD tests were performed at $\sigma'_{c0} = 50$ kPa, 100 kPa and 200 kPa, respectively. Sands and glass beads are not reused to avoid possible changes of particle shape or particle surface such as abrasion. Some important information including the initial void ratio e_0 , relative density, confining pressure and test type are summarized in Table 2.

3. Experimental results and analysis

3.1 Comparison of stress-strain and volume behavior in the PSC test

Developments of effective principal stress ratio and volumetric strain with the global axial strain ϵ_1 of the four types of material in the PSC test at $\sigma'_{c0} = 50$ kPa are compared in Fig. 6. Here, the principal stress ratio R is defined as σ'_1/σ'_3 , the ratio of effective vertical stress σ'_1 and effective confining stress σ'_3 . Clearly, all the materials gave typical results of dense granular materials showing gradually increasing strength until the peak and then softening. R shows high to low values from Ube No. 6A sand to Glassbead2. Dilation in Glassbead1 and Glassbead2 happened earlier than that in Toyoura sand, which is also earlier than that in Ube No. 6A sand. Dilation angle measured around the peak strength is 20.5°, 19.2°, 19.2° and 16.2° in the four types

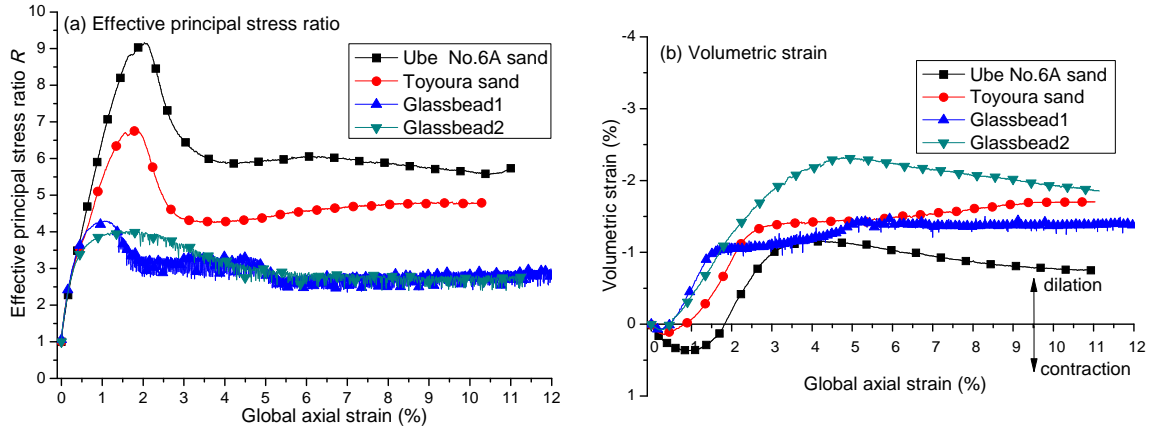


Fig. 6 Comparisons of stress-strain behavior of the four materials in the PSC test

of material, respectively. Here, the dilation angle is calculated by

$$\Psi = \sin^{-1} \left[\frac{(d\varepsilon_1^p + d\varepsilon_3^p)}{|(d\varepsilon_1^p + d\varepsilon_3^p)|} \right] \quad (1)$$

where ε_1^p and ε_3^p are the major and the minor plastic principal strains.

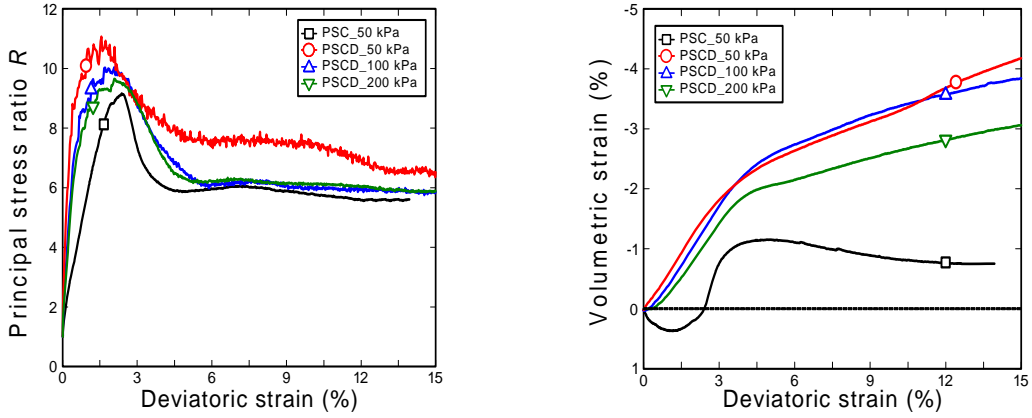
The Ube No. 6A sand with the most angular particle shape and lowest relative density showed the highest dilation angle. On the other hand, Toyoura sand and Glassbead1 with similar relative densities around 80% have the same dilation angle even if Toyoura sand has a more angular particle shape than Glassbead1. However, Ube No. 6A sand with the smallest dilation angle has the highest shear strength; Toyoura sand has higher shear strength than Glassbead1 even if they have the same dilation angle. This is because Ube No. 6A sand has the most angular particle shape and Toyoura sand has more angular particle shape than glass beads. Guo and Su (2007) have pointed out that interparticle locking owing to angularity contributes to a large part of the shear resistance of sands. Moreover, compared with Glassbead1, Glassbead2 clearly shows delayed peak strength and the curve from the peak to the residual state is less steep. This means the localization process is slower in Glassbead2 than that in Glassbead1. This is because shear band is thicker in Glassbead2 with larger particle size, which is discussed in detail in Section 4.

3.2 Test results in the PSCD test and comparison with PSC test

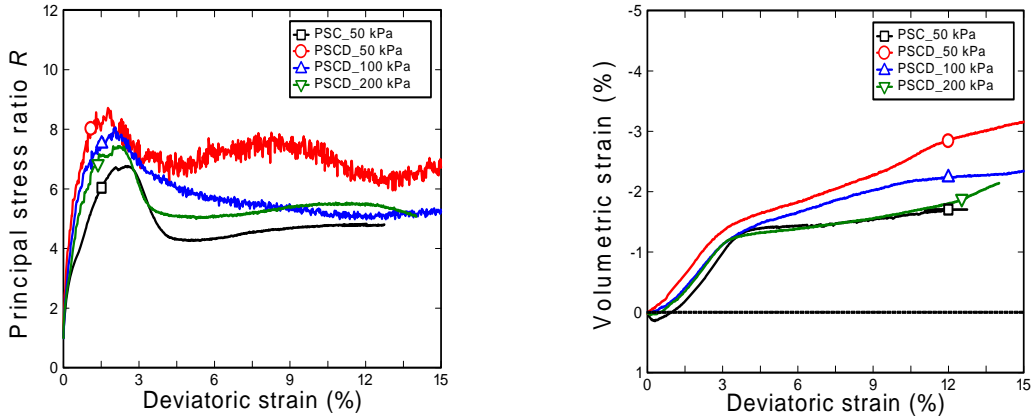
Test results of stress strain and volume behavior were summarized and compared in Fig. 7. The effective principal stress ratio R and volumetric strain were both plotted with the deviatoric strain. Here, the deviator strain ε_q is defined by

$$\varepsilon_q = \sqrt{\frac{2}{9}[(\varepsilon_1 - \varepsilon_2)^2 + (\varepsilon_2 - \varepsilon_3)^2 + (\varepsilon_3 - \varepsilon_1)^2]} \quad (2)$$

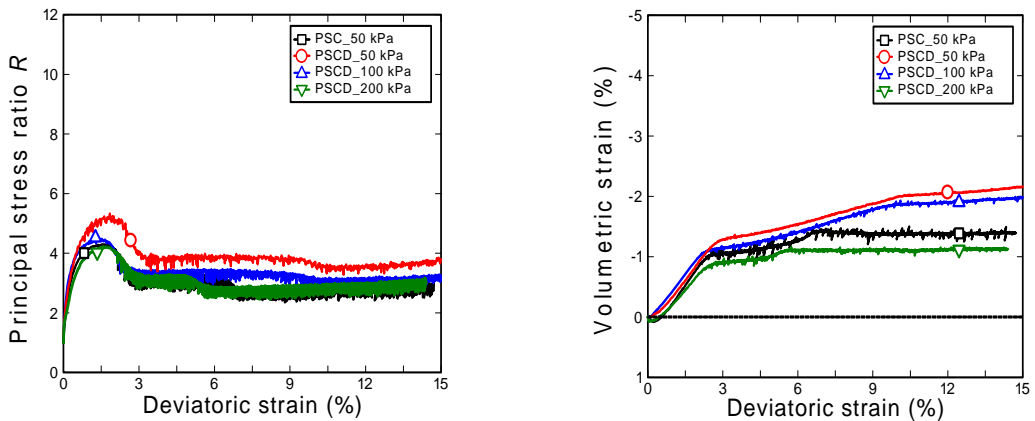
where ε_1 and ε_3 are approximated by the global vertical and lateral strain separately and $\varepsilon_2 = 0$.



(a) Ube No. 6A sand



(b) Toyoura sand



(c) Glassbead1

Fig. 7 Comparison of shear strength and volumetric strain behavior

It is found that there are significant differences between results of the two sands and the two glass beads. First is variation of peak strength with confining pressure in the three PSCD tests. The peak value of principal stress ratio, R_{\max} , in each case is listed in Table 2. In general, R_{\max} decreased with increasing stress level in both sands and glass beads. R_{\max} in glass beads is clearly higher under $\sigma'_{c0} = 50$ kPa while there is little variation when σ'_{c0} increased from 100 kPa to 200 kPa. It should also be noted that stick-slip of glass beads is more remarkable under higher stress level. Then, the peak appeared earlier with decreasing confining stress in the two sands but not in the glass beads. Moreover, the after-peak stress-strain behavior in the two sands varied differently under different test conditions while it always showed similar behavior in the two glass beads.

Stress path effect also behaved different between the sands and glass beads. All the three specimens in the PSCD test showed clearly higher stiffness (R/ε_q) before the peak, and earlier peak stress ratio than those in the PSC test for both the two sands. However, this was not found for the two glass beads. The $R - \varepsilon_q$ curves in the PSC test and in the two PSCD tests under $\sigma'_{c0} = 100$ kPa, 200 kPa almost overlapped in both the two glass beads.

The volume response in the PSCD test is a little different from that in the PSC test at the beginning of shearing. Different from the general volumetric change in dense granular material such as in Fig. 6(b), volume expansion happened in lieu of contraction due to stress release. Dilation developed gradually due to shearing and dilation angle reached the maximum value at the peak strength. It can also be known from Figs. 7(a) and (b) that before the peak strength, at the same global axial strain, total volumetric strains in the three PSCD tests are higher than that in the PSC test. Under the plane strain condition, this means more lateral extension was generated in the PSCD test than that in the PSC test for the two sands.

The dilation angles near the peak were listed in Table 2. It has been noted in past studies that the mobilized friction angle (or shear resistance) is contributed by several factors including inter particle friction, particle interlocking, dilation, particle rearrangement (Guo and Su 2007). However, it is not clear how much each factor contributes to the shear resistance. According to the angle values listed in Table 2, the dilation angle is found no more than 50% of the mobilized friction angle at the peak. The ratio of dilation angle and the maximum mobilized angle is 38-43% for Ube No. 6A sand, 34-40% for Toyoura sand, 43-50% for Glassbead1 and 38-44% for Glassbead2, respectively. The ratio is thought generally higher in glass beads than that in sands. Moreover, it is found that the dilation angle decreased with increasing consolidation pressure in the three PSCD tests, except that Glassbead2 showed the same value. The dilation angle decreased from 24.2° to 21.1° in Ube No. 6A sand, while it only changed 0.4° in Toyoura sand and 1.5° in Glassbead1. The Ube No. 6A sand with the most irregular particle shape is most vulnerable to stress level change.

From the above test results, it can be inferred that particle shape has a major influence on shear behavior, and the more angular particle shape makes the macro stress-strain behavior more sensitive to the stress level and stress path. Alshibli and Sture (2000) also noted that influence of confining pressure on strength and stability decreases as grain angularity decreases. In the subsequent sections, local deformation developments and shear band patterns in the specimens and particle shape effects are examined by image analysis.

4. Analysis and discussions of local deformations

Local deformation was observed in order to further understand the shear behavior. In this study,

we used the same photogrammetry method as introduced in detail by White *et al.* (2003). It is based on the PIV (Particle Image Velocity) method and the cross-correlation function is used to search new places of deformed materials. Therefore, it is also called DIC (Digital Image Correlation) method in many other studies; see for example a recent review by Hall *et al.* (2010). This method has been proven to be very useful to investigate shear band patterns (Desrues and Viggiani 2004, Rechenmacher and Finno 2004, Rechenmacher 2006). In order to improve luminance of the specimen, two 500-Watt LED lights were positioned in front of the observed window. A digital camera with a 35 mm of focal length was used and geometric correction was done to reduce the error induced by lens distortion. First, geometric correction is done by taking a photo of nodes range at a fixed spacing of 10 mm. About 300 nodes were included in a photo used for correction. The corrected pictures have a ratio of about 0.07-0.09 mm/pixel. Then, points of interest are selected inside the first photo and their coordinates are specified. A square standard pattern with a size of around 20*20 pixels is named based on each selected point (central point of the standard pattern). The mean gray scale of the standard pattern is calculated and is used as the base of judgment. Third, since locations of selected points changed in the next photo due to shear deformation, new positions of the points will be decided by searching new standard patterns having similar grey scale with previous ones. Here, a cross-correlation method is used, and the cross-correlation coefficient is calculated by

$$R_c = \frac{\sum_{j=0}^{N-1} \sum_{i=0}^{M-1} (f[i, j] - \bar{f})(s[i, j] - \bar{s})}{\sqrt{\sum_{j=0}^{N-1} \sum_{i=0}^{M-1} (f[i, j] - \bar{f})^2} \sqrt{\sum_{j=0}^{N-1} \sum_{i=0}^{M-1} (s[i, j] - \bar{s})^2}} \quad (3)$$

where, $f[i, j]$ is the grey scale of a single pixel in the standard pattern; \bar{f} is the mean grey scale of the standard pattern; $s[i, j]$ is the grey scale of a single pixel in the unknown pattern; \bar{s} is the mean grey scale of the unknown pattern; M, N is the pixel size of the decided standard pattern in the two directions.

When the new positions of the selected points are determined, the displacements of the selected points in the two dimensions of the plane are known. Finally, four-noded isotropic elements are used to solve strains inside the specimen based on the finite element method. Comparing the observed total displacement of specimen with the measured value by DIC analysis, it is found that the maximum error is no more than 0.6 mm within a total axial displacement of about 20 mm. Therefore, it is thought that this method has a high accuracy.

4.1 Local lateral deformation

It can be known from Fig. 7 that volumetric strain is higher in the PSCD test than that in the PSC test for sands. This means lateral strain is higher in the PSCD test under the plane strain condition. In order to verify this, local lateral strain distribution in specimen is investigated by DIC analysis at different stages of shearing. Fig. 9 shows comparisons of contour plots of Ube No. 6A sand and Glassbead2. The contours are compared at the same global axial strain ε_a in the PSC and PSCD test both under $\sigma'_{c0} = 50$ kPa. The ε_a is selected at an axial strain where peak is drawing near in the PSCD test. For the labels, '+' represents compression and '-' represents extension. It is found that local lateral deformation in specimen showed mainly extension. Butterfly-shaped

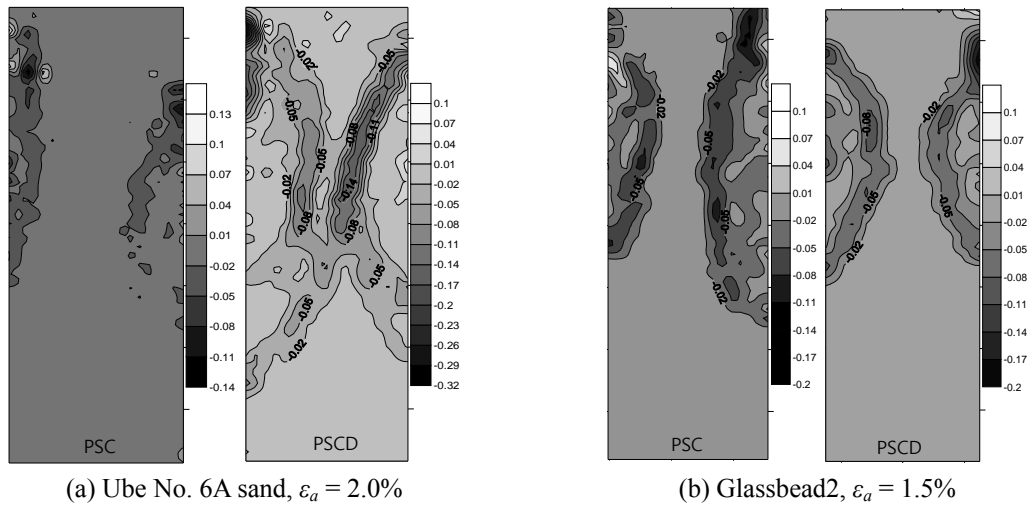


Fig. 8 Contour plots of local lateral strain

distribution was found in most specimens of both sand and glass beads. Amount of local extension in the PSC test is seen clearly less than that in the PSCD tests for Ube No. 6A sand, but not for Glassbead2. For example, as shown in Fig. 8(a), the maximum local later extension strain within shear band is about 0.15 in the PSC test of Ube No. 6A sand, while it is about 0.32 in the PSCD test. Moreover, the local deformation distribution is much narrower in the PSC test comparing with that in the PSCD test.

4.2 Shear band evolution and shear band thickness

Shear bands can be observed from local maximum shear strain distributions. This was also reported by Oda and Iwashita (2000). Here, the maximum shear strain is calculated by

$$\gamma_{\max} = \sqrt{(\epsilon_x - \epsilon_y)^2 + \gamma_{xy}^2} \tag{4}$$

where ϵ_x , ϵ_y , and γ_{xy} are the horizontal, vertical and shear strains of the divided elements in the observed plane, respectively.

According to the observations, double shear bands were finally generated in all the glass beads specimens, while both single and double shear bands were commonly found in sand specimens. For all the specimens under different test conditions, shear bands evolutions have similar but distinct ways. Shear bands developed with changing patterns during the whole shearing. The final shear bands are quite different from the initial ones, especially in sands. Fig. 9 shows a case of Toyoura sand in the PSCD test under $\sigma'_{c0} = 100$ kPa. Five stages were chosen including (a) at the peak, (b)-(d) typical stages and (e) at final state. It can be seen from Fig. 9(a) that several shear bands have been formed at the peak and they are quite nonuniform. Then, only the left-inclined band developed as shearing went on until 4.2% axial strain. After that the first shear band pattern had almost no change and a second shear band began to appear. The second one gradually evolved from discontinuous localized deformations and crossed with the first shear band. It grew wider and

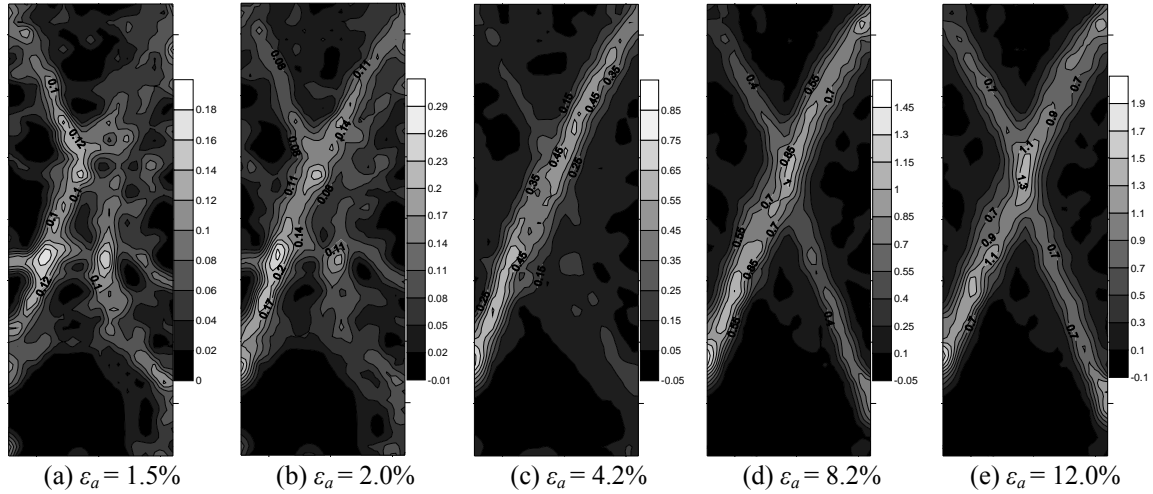


Fig. 9 Shear band evolutions in the PSCD test of Toyoura sand, $\sigma'_{c0} = 100$ kPa

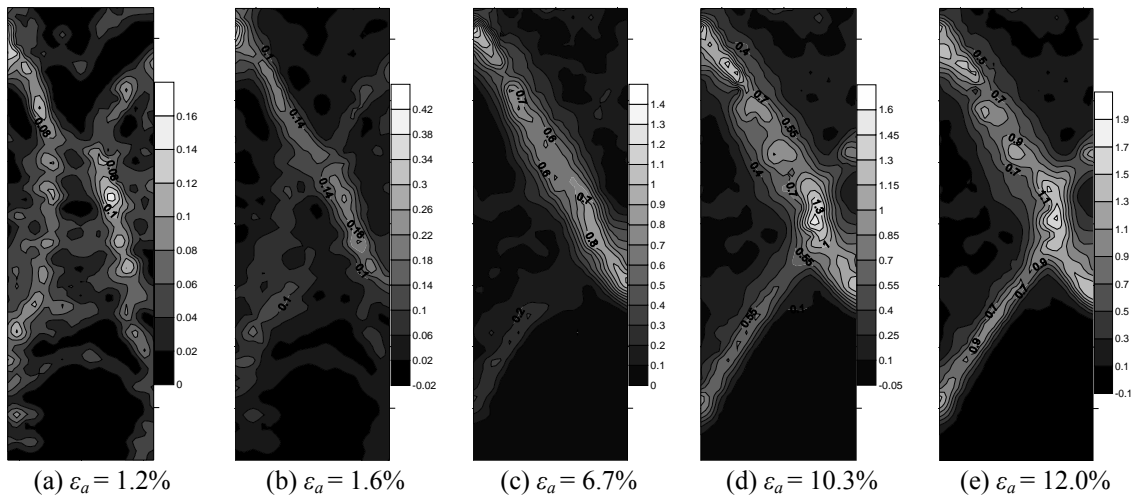


Fig. 10 Shear band evolutions in the PSCD test of Glassbead1, $\sigma'_{c0} = 100$ kPa

wider until the final state.

The above shear band evolutions are not limited to sands with irregular particle shapes. Similar case was also found in Glassbead1. Fig. 10 shows an example of the PSCD test under $\sigma'_{c0} = 100$ kPa. Symmetric shear bands have been formed at the peak with $\varepsilon_a = 1.2\%$, however they changed immediately and only one shear band was clearly observed at $\varepsilon_a = 1.6\%$. Then the shear band developed for a relatively long shearing period and a second shear band initiated at $\varepsilon_a = 6.7\%$. After that development in the first shear band almost ceased and increased deformation was localized within the second one until the final state.

Although two shear bands were finally formed in all the four cases of Glassbead1, they were not developed at the same time. The second shear band appeared at the under part of specimens as shown in Fig. 10 in two of the four cases, and it appeared at a symmetric location of the first one

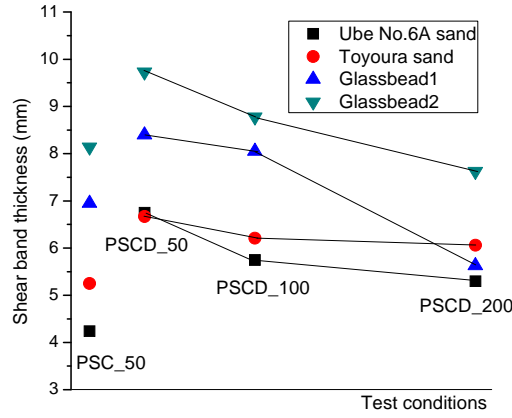


Fig. 11 Comparison of shear band thickness in the PSC and PSCD tests

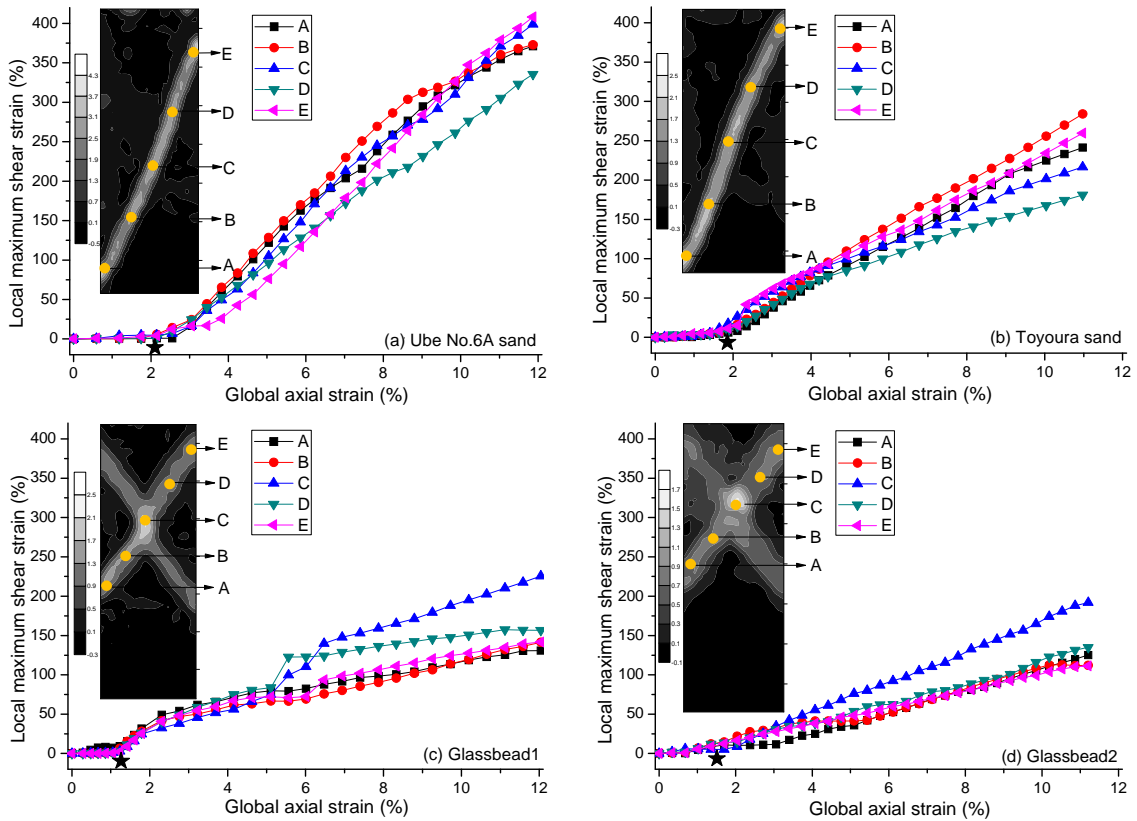


Fig. 12 Developments of local maximum shear strain: PSC test, $\sigma'_{c0} = 50$ kPa

in the other two cases (see Figs. 12(c) and 13(c)). Therefore, even for the Glassbead1 with very round particle shape and the relatively uniform narrow particle size distribution, shear bands are not always symmetric and they are hard to predict. However, for the Glassbead2 with almost five

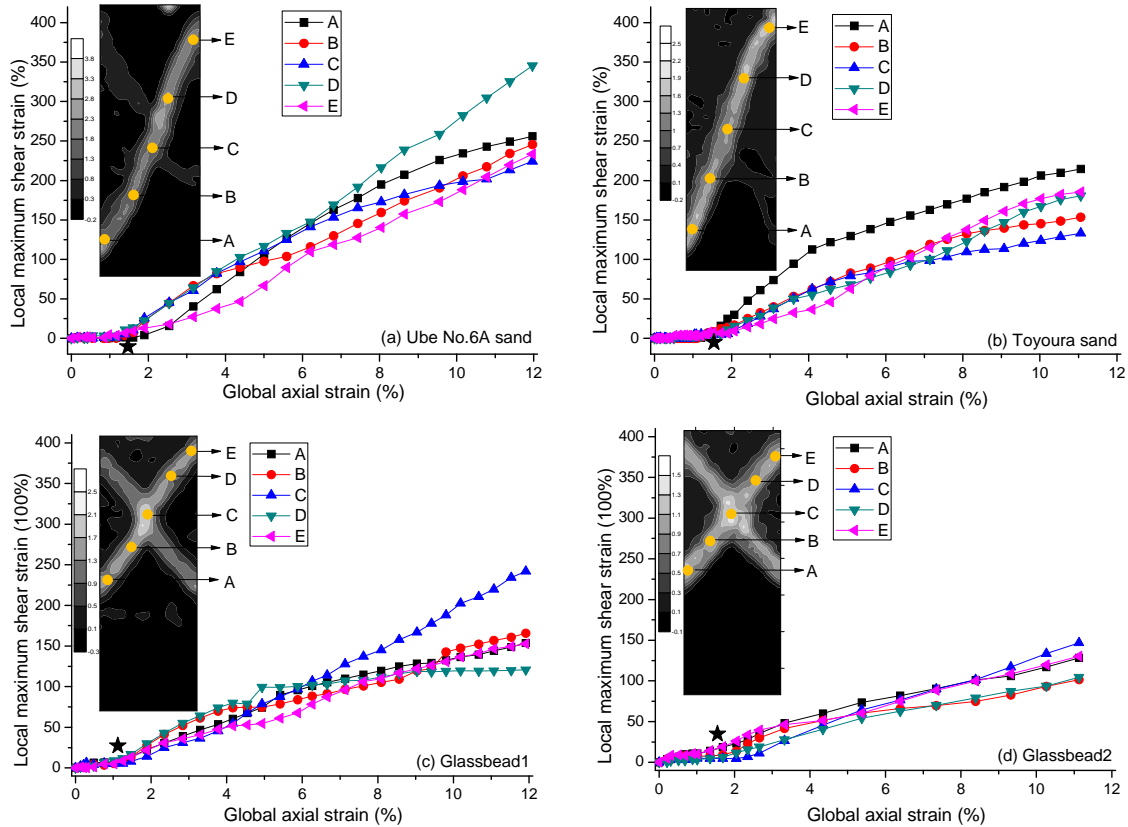


Fig. 13 Developments of local maximum shear strain: PSCD test, $\sigma'_{c0} = 200$ kPa

times of particle size of Glassbead1, symmetric and conjugate shear bands were always formed (see Figs. 12(d) and 13(d)).

From Figs. 9 and 10, it can be also seen that shear band is not perfectly uniform and its thickness changes at different places of the specimen. In order to make comparisons of shear band thickness in the four types of material, shear band thickness is measured at the middle height of the main shear band or it is measured slightly below the intersection for two conjugate shear bands. Fig. 11 shows measured results based on maximum shear strain contours for each case. The two sands and Glassbead1 have almost the same D_{50} , and Toyoura sand has very similar relative densities with Glassbead1, while their shear band thicknesses are not always similar. Glassbead1 has thicker shear band than the two sands. This is because Glassbead1 has a very uniform size distribution and round particle shape compared with the two sands. When comparing the two glass beads with the similar uniform size distribution but different particle size, Glassbead2 shows clear higher thickness than Glassbead1. However, the shear band thickness is not proportional to the mean particle size. The D_{50} size of Glassbead2 is almost 5 times as that of Glassbead1 while the ratio of their shear band thicknesses is only about 1.1-1.4 times. The ratio of shear band thickness and the D_{50} size is not constant for different granular materials and it decreases significantly when grain size becomes very big. This was also reported by Desrues and Viggiani (2004). Moreover, it is clearly seen that shear band thickness decreases with the increase of confining pressure in the

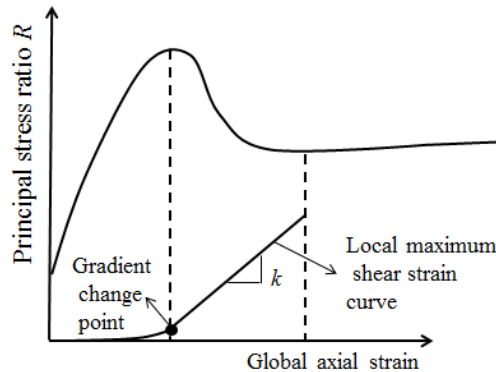


Fig. 14 Sketch of definition of growth rate k on the local maximum shear strain curve

PSCD test for all the materials.

4.3 Developments of local maximum shear strain within shear band

According to the above analysis, it is known that shear band is formed gradually and local deformations are not always uniform even within the same shear band. A direct way to identify these is to observe local strain developments within shear band. Fig. 12 shows the final shear band patterns and developments of local maximum shear strain with the global axial strain in the PSC tests under $\sigma'_{c0} = 50$ kPa. Fig. 13 shows the results in the PSCD tests under $\sigma'_{c0} = 200$ kPa. Five locations within the final main shear band at the ends of its quadrant are chosen, as marked by circular points in the figures. Local maximum shear strain variations at the locations are traced by the Lagrange method. As can be seen from the figures, maximum shear strains were very small and developed slowly at the beginning of shearing. As shearing continued, they began to increase stiffly at a certain global axial strain and gradient of the curve changed. This is therefore considered as the onset of shear band. The solid star symbol '★' in each subfigure in Figs. 12 and 13 shows the place of peak strength along axis of global axial strain. It can be seen that shear bands were formed just before or at peak strength.

Moreover, after the gradient change of the local maximum shear strain curve, the maximum shear strain within shear band grows approximately linearly with global axial strain. However, the rate of increase is not the same at the five locations especially for sands. As shown in Fig. 14, the growth rate is defined as $k = \Delta\gamma_{\max} / \Delta\varepsilon_a$ and it is measured by carrying out a linear approximation line to the local maximum shear strain curve between the start of gradient change and the end of softening.

Fig. 15 shows measured results in the PSC tests and Fig. 16 shows results in the PSCD tests under different confining pressures, respectively. For the same test case, some points overlapped because of the same growth rate of curves at different locations. The mean value of the five locations in each case was also given in the figures. In the PSC test results in Fig. 15, the growth rate decreased across the Ube No. 6A sand, Toyoura sand, Glassbead1 and Glassbead2. This is also found in the PSCD test results in Fig. 16. For each material, the average growth rate increased with increase of confining pressure. Moreover, the mean value of growth rate in most PSCD tests is seen lower than that in the PSC test for all the four types of material.

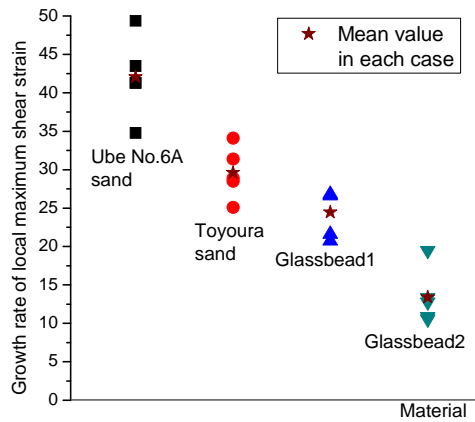


Fig. 15 Growth rate of maximum shear strain within shear band in the PSC tests

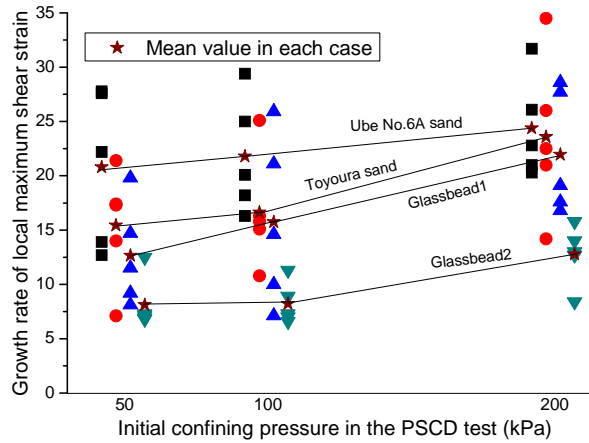


Fig. 16 Growth rate of maximum shear strain within shear band in the PSCD tests

Referring to the measured shear band thickness in Fig. 11, the above findings on the growth rate is thought related to shear band thickness. For the same material under different test conditions, it is clearly seen that the narrower of shear band the higher of growth rate. This inclination is also found when comparing different materials under the same test condition. According to the measured results in Figs. 15 and 16, for all the four sets of experiments in both PSC and PSCD tests, the growth rate is the highest in Ube No. 6A sand while it is the lowest in Glassbead2. The reason is that, for thicker shear band, it generates more displacements as local deformation reaching a certain extent of shear strain. As a result, the growth rate of maximum shear strain with global axial strain is lower.

4.4 Shear band inclination angle

Shear band inclination angle from the direction of the minor principal stress is often estimated by or compared with Coulomb's formula ($45^\circ + \varphi_m/2$), Roscoe's formula ($45^\circ + \Psi/2$) and Authur's formula ($45^\circ + \varphi_m/4 + \Psi/4$). Here, Ψ is the dilation angle given by Eq. (1) and φ_m is the mobilized

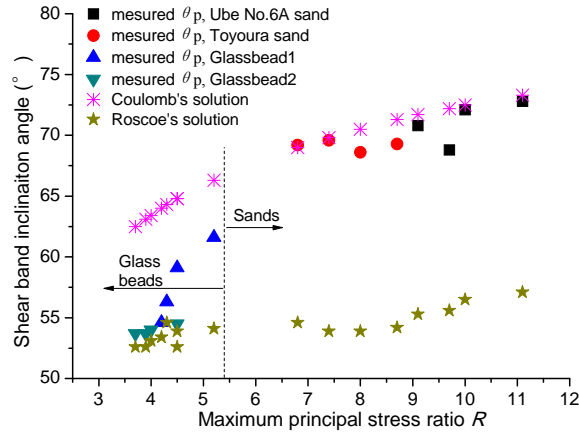


Fig. 17 Comparison of measured values and the classical solutions of shear band inclination angle

friction angle calculated according to the two principal stresses as

$$\varphi_m = \sin^{-1} \left[\frac{(\sigma'_1 - \sigma'_3)}{(\sigma'_1 + \sigma'_3)} \right]_{\max} \tag{5}$$

The observed inclination angles of shear band at the peak θ_p and at the residual state θ_r , and the two classical solutions were summarized in Table 2. These angles were measured at the middle part of the main shear band, and the highest value was taken if there are multiple main shear bands. Different comparison results were given by several researchers. Finno *et al.* (1997) concluded that the inclination angles in loose sands lied between Coulomb and Arthur solutions; measured results by Alshibli and Sture (2000) were much closer to Roscoe’s solution and the result was little influenced by relative density and particle size distribution. Fig. 17 shows comparison results on the horizontal axis of maximum principal stress ratio R . The R value was no more than 6 in the two glass beads and it was no less than 6 in the two sands. It is found that measured inclination angles in the two sands are well predicted by Coulomb’s formula with errors of 0-2°. For the two glass beads, measured values are quite close to Roscoe solutions in Glassbead2 while they lie between Coulomb solutions and Roscoe solutions in Glassbead1. As a result, Roscoe’s formula considering only dilation angle underestimated the shear band inclination angles in the sands, while Coulomb’s solution clearly overestimated the angles in the glass beads. The results revealed that the shear band inclination angle calculation method can be different between round and irregular granules. This needs more study in the future.

5. Conclusions

Plane strain compression tests with decreasing and constant confining pressure were performed on two sands and two glass beads under drained condition. Local deformations inside specimens were analyzed using the DIC method. Experimental results showed that particle shape has significant effects on shear behavior. Some detail conclusions are summarized as below:

- Macro stress – strain behavior is more easily influenced by stress level and stress path in the two sands than that in the two glass beads. The more angular particle shape induced more significant peak strength variations with stress level. For the given stress levels in this study, the peak appeared earlier and initial stiffness was clearly higher in all the PSCD tests than those in the PSC test for both the sands. The above differences were not found for the two glass beads.
- Local lateral strain showed mainly extension and butterfly shaped distribution near the peak strength. The extension was higher in the PSCD test than that in the PSC test for sands at the same global shear strain. Shear bands already initiated before peak strength and shear band pattern was changing during the whole shearing process.
- Under the same test condition, shear band thickness in the two sands was smaller than that in Glassbead1 even if they have almost the same mean particle size. The Ube No.6A sand with the most angular particle shape showed the lowest shear band thickness than the Toyoura sand and Glassbead1 under the same test condition. Shear band thickness decreased with increase of confining pressure regardless of particle shape or size.
- When shear band initiated, local maximum shear strain starts to increase stiffly. The local maximum shear strain inside shear band grew approximately linearly with global axial strain from onset of shear band to the end of softening. The growth rate was found to be related to shear band thickness. The wider shear band, the relatively lower the growth rate.
- The Coulomb's formula gave pretty good predictions of shear band inclination angle for the two sands but much overestimated the two glass beads. Shear band inclination angles were quite close to Roscoe solutions in Glassbead2 while they lied between Coulomb and Roscoe solutions in Glassbead1.

Acknowledgments

The authors thank Messrs. Kajiwara and Namihira of Yamaguchi University for their help in the experiments.

References

- Alshibli, K.A. and Sture, S. (2000), "Shear band formation in plane strain experiments of sand", *J. Geotech. Geoenviron. Eng.*, **126**(6), 495-503.
- Alshibli, K.A. and Alsaleh, M.I. (2004), "Characterizing surface roughness and shape of sands using digital microscopy", *J. Comput. Civil. Eng.*, **18**(1), 36-45.
- Cho, G.C., Dodds, J. and Santamarina, J.C. (2006), "Particle Shape Effects on Packing Density, Stiffness, and Strength: Natural and Crushed Sands", *J. Geotech. Geoenviron. Eng.*, **132**(5), 591-602.
- Chu, J., Leong, W.K., Loke, W.L. and Wanatowski, D. (2012), "Instability of loose sand under drained conditions", *J. Geotech. Geoenviron. Eng.*, **138**(2), 207-216.
- Chu, J. and Wanatowski, D. (2009), "Effect of loading mode on strain softening and instability behavior of sand in plane-strain test", *J. Geotech. Geoenviron. Eng.*, **135**(1), 108-120.
- Desrues, J. and Viggiani, G. (2004), "Strain localization in sand: an overview of the experimental results obtained in Grenoble using stereophotogrammetry", *Int. J. Numer. Anal. Method. Geomech.*, **28**, 279-321.
- Finno, R.J., Harris, W.W., Mooney, M.A. and Viggiani, G. (1997), "Shear bands in plane strain compression of loose sand", *Géotechnique*, **47**(1), 149-165.
- Guo, P.J. and Stolle, D.F.E. (2005), "On the failure of granular material with fabric effects", *Soils Found.*, **45**(4), 1-12.

- Guo, P.J. and Su, X.B. (2007), "Shear strength, interparticle locking, and dilatancy of granular materials", *Can. Geotech. J.*, **44**(5), 579-591
- Hall, S.A., Bornert, M., Desrues, J., Pannier, Y., Lenoir, N., Viggiani, G. and Bésuelle, P. (2010), "Discrete and continuum analysis of localised deformation in sand using X-ray μ CT and volumetric digital image correlation", *Géotechnique*, **60**(5), 315-322.
- Head, K.H. (1992), *Effective Stress Tests – Manual of Soil Laboratory Testing*, (2nd Edition), Vol. 3, Pentech Press, London.
- Katagiri, J., Matsushima, T. and Yamada, Y. (2010), "Simple shear simulation of 3D irregularly-shaped particles by image-based DEM", *Granular Matter*, **12**, 491-497.
- Maeda, K., Sakai, H., Kondo, A., Yamaguchi, T., Fukuma, M. and Nukudani, E. (2010), "Stress-chain based micromechanics of sand with grain shape effect", *Granul. Matter*, **12**(5), 499-505.
- Masuda, T., Tatsuoka, F., Yamada, S. and Sato, T. (1999), "Stress-strain behavior of sand in plane strain compression, extension and cyclic loading tests", *Soils Found.*, **39**(5), 31-45.
- Matsushima, T. and Chang, C.S. (2011), "Quantitative evaluation of the effect of irregularly shaped particles in sheared granular assemblies", *Granul. Matter*, **13**(3), 269-276.
- Oda, M. and Iwashita, K. (2000), "Study on couple stress and shear band development in granular media based on numerical simulation analyses", *Int. J. Eng. Sci.*, **38**(15), 1713-1740.
- Rechenmacher, A.L. (2006), "Grain-scale process governing shear band initiation and evolution in sands", *J. Mech. Phys. Solids*, **54**(1), 22-45.
- Rechenmacher, A.L. and Finno, R.J. (2004), "Digital image correlation to evaluate shear banding in dilative sands", *Geotech. Test. J.*, **27**(1), 13-22.
- Röchter, L., König, D., Schanz, T. and Triantafyllidis, T. (2010), "Shear banding and strain softening in plane strain extension, physical modeling", *Granular Matter*, **12**(3), 287-301.
- Röchter, L., König, D., Schanz, T., Niemunis, A. and Triantafyllidis, T. (2011), "Shear band systems in plane strain extension: analytical solution and comparison with experimental results", *Granul. Matter*, **13**(5), 553-563.
- Sezer, A., Altun, S. and Göktepe, B.A. (2011), "Relationships between shape characteristics and shear strength of sands", *Soils Found.*, **51**(5), 857-871.
- Shinohara, K., Oida, M. and Golman, B. (2000), "Effect of particle shape on angle of internal friction by triaxial compression test", *Powder Technol.*, **107**(1-2), 131-136.
- Tatsuoka, F., Nakamura, S., Huang, C.C. and Tani, K. (1990), "Strength anisotropy and shear band direction in plane strain tests of sand", *Soils Found.*, **30**(1), 35-54.
- Tejchman, J., Bauer, E. and Wu, W. (2007), "Effect of fabric anisotropy on shear localization in sand during plane strain compression", *Acta Mechanica*, **189**(1-4), 23-51.
- Wanatowski, D. and Chu, J. (2006), "Stress-strain behavior of a granular fill measured by a new plane-strain apparatus", *Geotech. Test. J.*, **29**(2), 149-157.
- Wanatowski, D., Chu, J. and Loke, W.L. (2010), "Drained instability of sand in plane strain", *Can. Geotech. J.*, **47**(4), 400-412.
- White, D.J., Take, W.A. and Bolton, M.D. (2003), "Soil deformation measurement using particle image velocimetry (PIV) and photogrammetry", *Géotechnique*, **53**(7), 619-631.